

# Improving Gate-Level Simulation of Quantum Circuits\*

George F. Viamontes, Igor L. Markov, and John P. Hayes  
{gviamont, imarkov, jhayes}@eecs.umich.edu

The University of Michigan, Advanced Computer Architecture Laboratory  
Ann Arbor, MI 48109-2122, USA

October 16, 2019

## Abstract

Simulating quantum computation on a classical computer is a difficult problem. The matrices representing quantum gates, and vectors modeling qubit states grow exponentially with an increase in the number of qubits. However, by using a novel data structure called the Quantum Information Decision Diagram (QuIDD) that exploits the structure of quantum operators, many of these matrices and vectors can be represented in a form that grows polynomially with an increase in the number of qubits. Using QuIDDs, we implemented a general-purpose quantum computing simulator in C++ called QuIDDPro and tested it on Grover's algorithm. Our QuIDD technique asymptotically outperforms other known simulation techniques.

arXiv:quant-ph/0309060v1 6 Sep 2003

---

\*Earlier results of this work were reported at ASPDAC '03 [18]. New material includes significantly better experimental results and a description of a large class of matrices and vectors which can be manipulated in polynomial time and memory using QuIDDPro.

# 1 Introduction

Richard Feynman observed in the 1980s that simulating quantum mechanical processes on a standard *classical* computer seems to require super-polynomial memory and time [12]. For instance, a complex vector of size  $2^n$  is needed to represent all the information in  $n$  quantum states, and square matrices of size  $2^{2n}$  are needed to model (simulate) the time evolution of the states [14]. Consequently, Feynman proposed *quantum computing* which uses the quantum mechanical states themselves to simulate quantum processes. The key idea is to replace bits with quantum states called *qubits* as the fundamental units of information. A quantum computer can operate directly on exponentially more data than a classical computer with a similar number of operations and information units. Thus in addressing the problem of simulating quantum mechanical processes more efficiently, Feynman discovered a new computing model that can outperform classical computation in certain cases.

Software simulation has long been an invaluable tool for the design and testing of digital circuits. This problem too was once thought to be computationally intractable. Early simulation and synthesis techniques for  $n$ -bit circuits often required  $O(2^n)$  runtime and memory, with the worst-case complexity being fairly typical. Later algorithmic advancements brought about the ability to perform circuit simulation much more efficiently in practical cases. One such advance was the development of a data structure called the Reduced Ordered Binary Decision Diagram (ROBDD) [5], which can greatly compress the Boolean description of digital circuits and allow direct manipulation of the compressed form. Software simulation may also play a vital role in the development of quantum hardware by enabling the modeling and analysis of large-scale designs that cannot be implemented physically with current technology. Unfortunately, straightforward simulation of quantum designs by classical computers executing standard linear-algebraic routines requires  $O(2^n)$  time and memory [12, 14]. However, just as ROBDDs and other innovations have made the simulation of very large classical computers tractable, new algorithmic techniques can allow the efficient simulation of quantum computers.

The goal of the work reported here is to develop a practical software means of simulating quantum computers efficiently on classical computers. We propose a new data structure called the *Quantum Information Decision Diagram* (QuIDD) which is based on decision diagram concepts that are well-known in the context of simulating classical computer hardware [6, 2, 5]. As we demonstrate, QuIDDs allow simulations of  $n$ -qubit systems to achieve run-time and memory complexities that range from  $O(1)$  to  $O(2^n)$ , and the worst case is not typical. In the important case of Grover’s quantum search algorithm [11], we show that our QuIDD-based simulator outperforms all other known simulation techniques.

The paper is organized as follows. Section 2 outlines previous work on decision diagrams and the modeling of quantum computation on classical computers. In Section 3 we present our QuIDD data structure. Section 4 analyzes the runtime and memory complexity of QuIDD operations, while Section 5 describes some experimental results using QuIDDs. Finally, in Section 6 we present our conclusions and ideas for future work.

## 2 Background

This section first presents the basic concepts of decision diagrams, assuming only a rudimentary knowledge of computational complexity and graph theory. It then reviews previous research on simulating quantum mechanical matrix operations.

### 2.1 Binary Decision Diagrams

The binary decision diagram (BDD) was introduced by Lee in 1959 [13] in the context of classical logic circuit design. This data structure represents a Boolean function  $f(x_1, x_2, \dots, x_n)$  by a directed acyclic graph (DAG); see Figure 1. By convention, the top node of a BDD is labeled with the name of the function  $f$  represented by the BDD. Each variable  $x_i$  of  $f$  is associated with one or more nodes with two outgoing edges labeled *then* (solid line) and *else* (dashed line). The *then* edge of node  $x_i$  denotes an assignment of logic 1 to the  $x_i$ , while the *else* edge represents an assignment of logic 0. These nodes are called *internal nodes* and are labeled by the corresponding variable  $x_i$ . The edges of the BDD point downward, implying a top-down assignment of values to the Boolean variables depicted by the internal nodes.

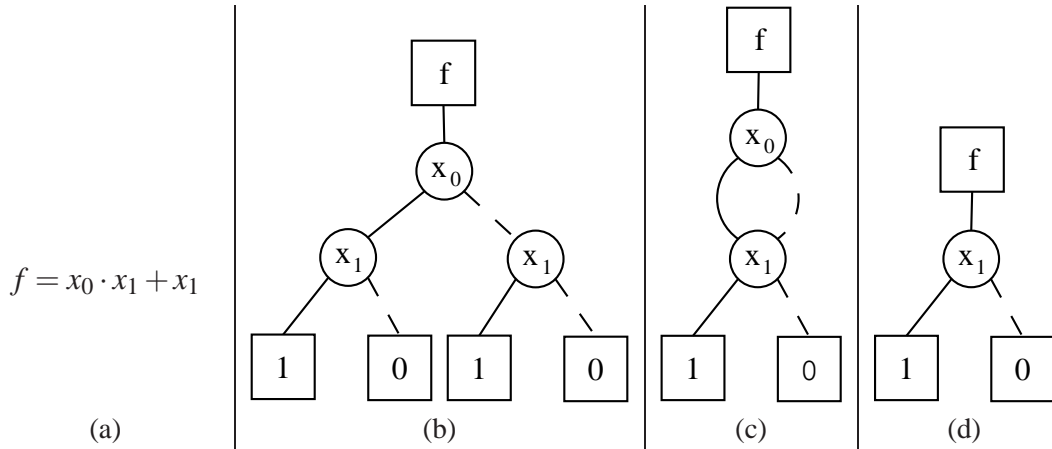


Figure 1: (a) A logic function, (b) its BDD representation, (c) its BDD representation after applying the first reduction rule, and (d) its ROBDD representation.

At the bottom of the BDD are *terminal* nodes containing the logic values 1 or 0. They denote the output value of the function  $f$  for a given assignment of its variables. Each path through the BDD from top to bottom represents a specific assignment of 0-1 values to the variables  $x_1, x_2, \dots, x_n$  of  $f$ , and ends with the corresponding output value  $f(x_1, x_2, \dots, x_n)$ .

The original BDD data structure conceived by Lee has exponential worst-case memory complexity  $\Theta(2^n)$ , where  $n$  is the number of Boolean variables in a given logic function. Moreover, exponential memory is required in many cases, making this data structure impractical for simulation of large logic circuits. To address this limitation, Bryant developed the Reduced Ordered BDD (ROBDD) [5]. A key advantage of the ROBDD is its use of certain reduction rules. These rules automatically eliminate redundancy from the basic BDD representation and may be summarized as follows:

1. There are no nodes  $v$  and  $v'$  such that the subgraphs rooted at  $v$  and  $v'$  are isomorphic
2. There are no internal nodes with *then* and *else* edges that both point to the same node

An example of how the rules transform a BDD into an ROBDD is shown in Figures 1c and 1d. The subgraphs rooted at the  $x_1$  nodes in Figure 1b are isomorphic. By applying the first reduction rule, the BDD in Figure 1b is converted into the BDD in Figure 1c. Notice that in this new BDD, the *then* and *else* edges of the  $x_0$  node now point to the same node. Applying the second reduction rule eliminates the  $x_0$  node, producing the ROBDD in Figure 1d. Intuitively it makes sense to eliminate the  $x_0$  node since the output of the original function is determined solely by the value of  $x_1$ .

Another aspect of redundancy elimination is the order in which variables are evaluated in an ROBDD. Different variable orderings can lead to drastic differences in ROBDD size, and finding the optimal variable ordering is an *NP*-complete problem. It turns out, however, that many practical logic functions have ROBDD representations that are either linear or polynomial in the number of input variables [5]. ROBDDs therefore offer a much more efficient representation for logic circuits than do unreduced BDDs or truth-tables; both of which are exponential in the number of input variables.

## 2.2 BDD Operations

Even though the ROBDD is often quite compact, efficient algorithms are necessary to make it practical for circuit simulation. Thus, in addition to the foregoing reduction rules, Bryant introduced a variety of ROBDD operations whose complexities are bounded by the size of the ROBDDs being manipulated [5]. Of central importance is the *Apply* operation, which performs a binary operation with two ROBDDs, producing a third ROBDD as the result. It can be used, for example, to compute the logical *AND* of two functions. *Apply* is implemented by a recursive traversal of the two ROBDD operands. For each pair of nodes visited during the traversal, an internal node is added to the resultant ROBDD using the three rules depicted in Figure 2. To

understand the rules, some notation must be introduced. Let  $v_f$  denote an arbitrary node in an ROBDD  $f$ . If  $v_f$  is an internal node,  $Var(v_f)$  is the Boolean variable represented by  $v_f$ ,  $T(v_f)$  is the node reached when traversing the *then* edge of  $v_f$ , and  $E(v_f)$  is the node reached when traversing the *else* edge of  $v_f$ .

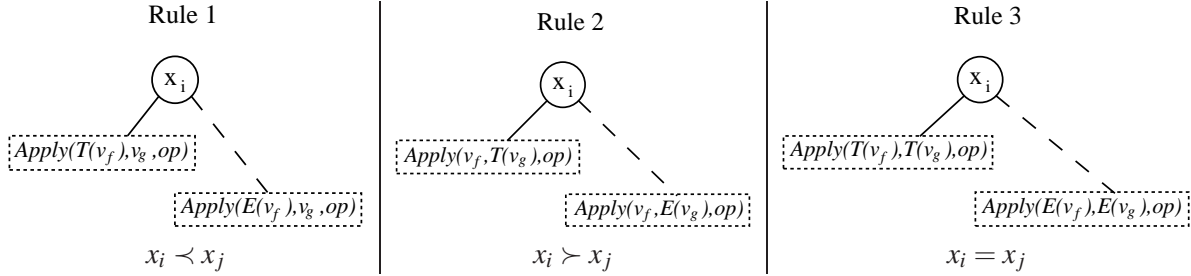


Figure 2: The three recursive rules used by the *Apply* operation which determine how a new node should be added to a resultant ROBDD. In the figure,  $x_i = Var(v_f)$  and  $x_j = Var(v_g)$ . The notation  $x_i < x_j$  is defined to mean that  $x_i$  precedes  $x_j$  in the variable ordering.

Clearly the rules depend on the variable ordering. To illustrate, consider performing *Apply* using a binary operation  $op$  and two ROBDDs  $f$  and  $g$ . *Apply* takes as arguments two nodes, one from  $f$  and one from  $g$ , and the operation  $op$ . This is denoted as  $Apply(v_f, v_g, op)$ . *Apply* compares  $Var(v_f)$  and  $Var(v_g)$  and adds a new internal node to the ROBDD result using the three rules. The rules also guide *Apply*'s traversal of the *then* and *else* edges (this is the recursive step). For example, suppose  $Apply(v_f, v_g, op)$  is called and  $Var(v_f) < Var(v_g)$ . Rule 1 is invoked, causing an internal node containing  $Var(v_f)$  to be added to the resulting ROBDD. Rule 1 then directs the *Apply* operation to call itself recursively with  $Apply(T(v_f), v_g, op)$  and  $Apply(E(v_f), v_g, op)$ . Rules 2 and 3 dictate similar actions but handle the cases when  $Var(v_f) > Var(v_g)$  and  $Var(v_f) = Var(v_g)$ . To recurse over both ROBDD operands correctly, the initial call to *Apply* must be  $Apply(Root(f), Root(g), op)$  where  $Root(f)$  and  $Root(g)$  are the root nodes for the ROBDDs  $f$  and  $g$ .

The recursion stops when both  $v_f$  and  $v_g$  are terminal nodes. When this occurs,  $op$  is performed with the values of the terminals as operands, and the resulting value is added to the ROBDD result as a terminal node. For example, if  $v_f$  contains the value logical 1,  $v_g$  contains the value logical 0, and  $op$  is defined to be  $\oplus$  (*XOR*), then a new terminal with value  $1 \oplus 0 = 1$  is added to the ROBDD result. Terminal nodes are considered *after* all variables are considered. Thus, when a terminal node is compared to an internal node, either Rule 1 or Rule 2 will be invoked depending on which ROBDD the internal node is from.

ROBDD variants have been adopted in several contexts outside the domain of logic design. Of particular relevance to this work are Multi-Terminal Binary Decision Diagrams (MTBDDs) [6] and Algebraic Decision Diagrams (ADDs) [2]. These data structures are compressed representations of matrices and vectors rather than logic functions, and the amount of compression achieved is proportional to the frequency of repeated values in a given matrix or vector. Additionally, some standard linear-algebraic operations, such as matrix multiplication, are defined for MTBDDs and ADDs. Since they are based on the *Apply* operation, the efficiency of these operations is proportional to the size in nodes of the MTBDDs or ADDs being manipulated. Further discussion of the MTBDD and ADD representations is deferred to Subsection 3.1 where the general structure of the QuIDD is described.

## 2.3 Previous Linear-Algebraic Techniques

Quantum-circuit simulators must support linear-algebraic operations such as matrix multiplication, the tensor product, and the projection operators. They typically employ array-based methods to multiply matrices and so require exponential computational resources in the number of qubits. Such methods are often insensitive to the actual values stored, and even sparse-matrix storage offers little improvement for quantum operators with no zero matrix elements, such as Hadamard operators.

Several clever matrix methods have been developed for quantum simulation. For example, one can simulate  $k$ -input quantum gates on an  $n$ -qubit state vector ( $k \leq n$ ) without explicitly storing a  $2^n \times 2^n$ -matrix representation. The basic idea is to simulate the full-fledged matrix-vector multiplication by a series of simpler operations. To illustrate, consider simulating a quantum circuit in which a 1-qubit Hadamard

operator is applied to the third qubit of the state-space  $|00100\rangle$ . The state vector representing this state-space has  $2^{32}$  elements. A naive way to apply the 1-qubit Hadamard is to construct a  $2^{32} \times 2^{32}$  matrix of the form  $I \otimes I \otimes H \otimes I \otimes I$  and then multiply this matrix by the state vector. However, rather than compute  $(I \otimes I \otimes H \otimes I \otimes I)|00100\rangle$ , one can simply compute  $|00\rangle \otimes H|1\rangle \otimes |00\rangle$ , which produces the same result using a  $2 \times 2$  matrix  $H$ . The same technique can be applied when the state-space is in a superposition, such as  $\alpha|00100\rangle + \beta|00000\rangle$ . In this case, to simulate the application of a 1-qubit Hadamard operator to the third qubit, one can compute  $|00\rangle \otimes H(\alpha|1\rangle + \beta|0\rangle) \otimes |00\rangle$ . As in the previous example, a  $2 \times 2$  matrix is sufficient.

While the above method allows one to compute a state space symbolically, in a realistic simulation environment, state vectors may be much more complicated. Shortcuts that take advantage of the linearity of matrix-vector multiplication are desirable. For example, a single qubit can be manipulated in a state vector by extracting a certain set of two-dimensional vectors. Each vector in such a set is composed of two probability amplitudes. The corresponding qubit states for these amplitudes differ in value at the position of the qubit being operated on but agree in every other qubit position. The two-dimensional vectors are then multiplied by matrices representing single qubit gates in the circuit being simulated. We refer to this technique as *qubit-wise multiplication* because the state-space is manipulated one qubit at a time. Obenland implemented a technique of this kind as part of a simulator for quantum circuits [15]. His method applies one- and two-qubit operator matrices to state vectors of size  $2^n$ . Unfortunately, in the best case where  $k = 1$ , this only reduces the runtime and memory complexity from  $O(2^{2n})$  to  $O(2^n)$ , which is still exponential in the number of qubits.

Gottesman developed a simulation method involving the *Heisenberg representation* of quantum computation which tracks the commutators of operators applied by a quantum circuit [9]. With this model, the state vector need not be represented explicitly because the operators describe how an arbitrary state vector would be altered by the circuit. Gottesman showed that simulation based on this model requires only polynomial memory and runtime on a classical computer in certain cases. However, it appears limited to the Clifford and Pauli groups of quantum operators, which do not form a universal gate library.

Other advanced simulation techniques including MATLAB’s “packed” representation, apply data compression to matrices and vectors, but cannot perform matrix-vector multiplication on compressed matrices and vectors. A notable exception is Greve’s simulation of Shor’s algorithm that uses BDDs [10]. Probability amplitudes of individual qubits are modeled by single decision nodes. This only captures superpositions where every participating qubit is rotated by  $\pm 45$  degrees from  $|0\rangle$  toward  $|1\rangle$ . Another BDD-based technique was recently proposed by Al-Rabadi et al. [1] which can perform multi-valued quantum logic. A drawback of this technique is that it is used for *synthesis* of quantum logic gates rather than simulation of their behavior.

Though Greve’s and Al-Rabadi et al.’s BDD representations cannot simulate arbitrary quantum circuits, the idea of modeling quantum states with a BDD-based structure is appealing and motivates our approach. Unlike previous techniques, our approach is capable of simulating arbitrary quantum circuits while offering performance improvements as demonstrated by the results presented in Sections 4 and 5.

### 3 QuIDD Theory

The *Quantum Information Decision Diagram* (QuIDD) was born out of the observation that vectors and matrices which arise in quantum computing exhibit repeated structure. Complex operators obtained from the tensor product of simpler matrices continue to exhibit common substructures which certain BDD variants can capture. MTBDDs and ADDs, introduced in Subsection 2.2, are particularly relevant to the task of simulating quantum systems. The QuIDD can be viewed as an ADD or MTBDD with the following properties:

1. The values of terminal nodes are restricted to the set of complex numbers
2. Rather than contain the values explicitly, QuIDD terminal nodes contain integer indices which map into a separate array of complex numbers. This allows the use of a simpler integer function for *Apply*-based operations, along with existing ADD and MTBDD libraries [17], greatly reducing implementation overhead.
3. The variable ordering of QuIDDs interleaves row and column variables, which favors compression of block patterns (see Subsection 3.2)

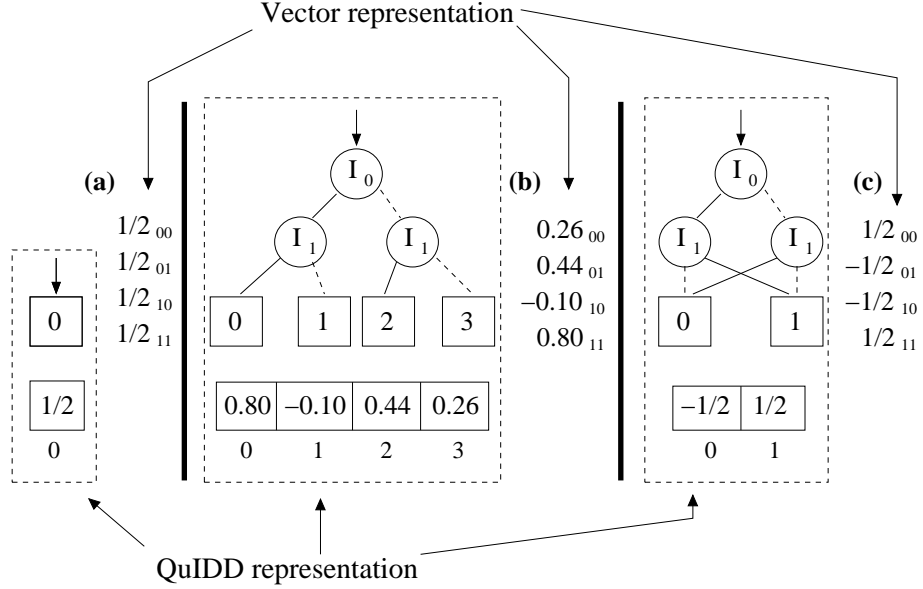


Figure 3: Sample QuIDDs for state vectors of (a) best, (b) worst and (c) mid-range size.

4. Bahar et al. note that ADDs can be padded with 0's to represent arbitrarily sized matrices [2]. No such padding is necessary in the quantum domain where all vectors and matrices have sizes that are a power of 2 (see Subsection 3.2)

As we demonstrate using our QuIDD-based simulator, called QuIDDPro, these properties greatly enhance performance of quantum computational simulation.

### 3.1 Vectors and Matrices

Figure 3 shows the QuIDD structure for three 2-qubit states. We consider the indices of the four vector elements to be binary numbers, and define their bits as decision variables of QuIDDs. A similar definition is used for ADDs [2]. For example, traversing the *then* edge (solid line) of node  $I_0$  in Figure 3c is equivalent to assigning the value 1 to the first bit of the 2-bit vector index. Traversing the *else* edge (dotted line) of node  $I_1$  in the same figure is equivalent to assigning the value 0 to the second bit of the index. These traversals bring us to the terminal value  $-\frac{1}{2}$ , which is precisely the value at index 10 in the vector representation.

QuIDD representations of matrices extend those of vectors by adding a second type of variable node and enjoy the same reduction rules and compression benefits. Consider the 2-qubit Hadamard matrix annotated with binary row and column indices shown in Figure 4a. In this case there are two sets of indices: The first (vertical) set corresponds to the rows, while the second (horizontal) set corresponds to the columns. We assign the variable name  $R_i$  and  $C_j$  to the row and column index variables respectively. This distinction between the two sets of variables was originally noted in several works including that of Bahar et al. [2]. Figure 4b shows the QuIDD form of this sample matrix where it is used to modify the state vector  $|00\rangle = (1, 0, 0, 0)$  via matrix-vector multiplication, an operation discussed in more detail in Subsection 3.4.

### 3.2 Variable Ordering

As explained in Subsection 2.1, variable ordering can drastically affect the level of compression achieved in BDD-based structures such as QuIDDs. The CUDD programming library [17], which is incorporated into QuIDDPro, offers sophisticated dynamic variable-reordering techniques that achieve performance improvements in various BDD applications. However, dynamic variable reordering has significant time overhead, whereas finding a good static ordering in advance may be preferable in some cases. Good variable orderings are highly dependent upon the structure of the problem at hand, and therefore one way to seek out a good ordering is to study the problem domain. In the case of quantum computing, we notice that all matrices

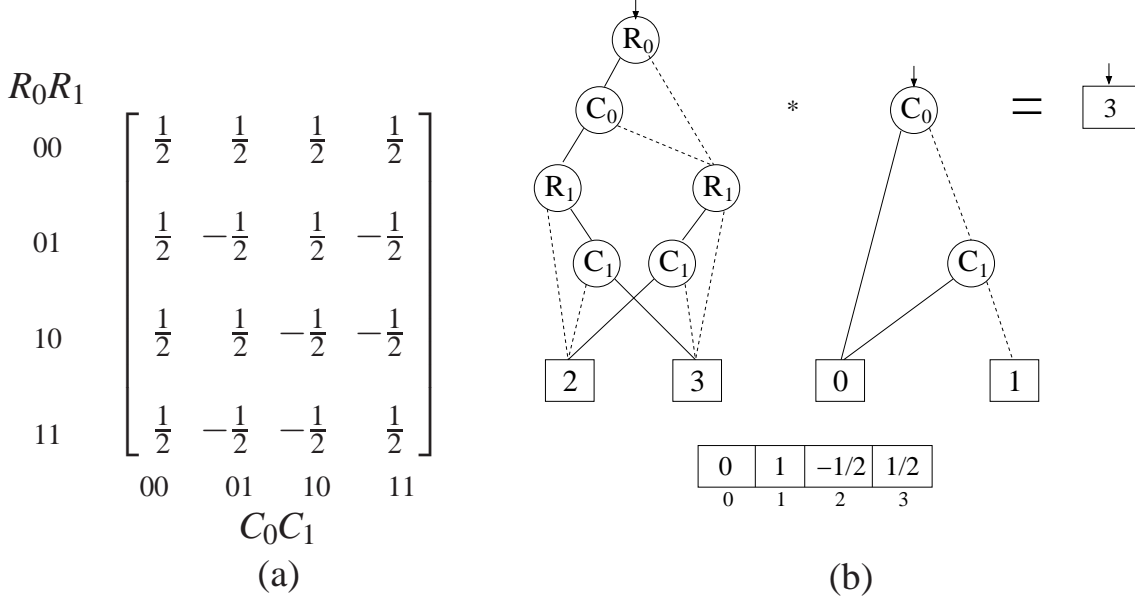


Figure 4: (a) 2-qubit Hadamard, and (b) its QuIDD representation multiplied by  $|00\rangle = (1, 0, 0, 0)$ . Note that the vector and matrix QuIDDs share the entries in a terminal array that is global to the computation.

and vectors contain  $2^n$  elements where  $n$  is the number of qubits represented. Additionally, the matrices are square and non-singular [14].

McGeer et al. demonstrated that ADDs representing certain rectangular matrices can be operated on efficiently with interleaved row and column variables [7]. Interleaving implies the following variable ordering:  $R_0 \prec C_0 \prec R_1 \prec C_1 \prec \dots \prec R_n \prec C_n$ . Intuitively, the interleaved ordering causes compression to favor regularity in block sub-structures of the matrices. We observe that such regularity is created by tensor products that are required to allow multiple quantum gates to operate in parallel and also to extend smaller quantum gates to operate on larger numbers of qubits. The tensor product  $A \otimes B$  multiplies each element of  $A$  by the whole matrix  $B$  to create a larger matrix which has dimensions  $M_A \cdot M_B$  by  $N_A \cdot N_B$ . By definition, the tensor product will propagate block patterns in its operands. To illustrate the notion of block patterns and how QuIDDs take advantage of them, consider the tensor product of two one-qubit Hadamard operators:

$$\left[ \begin{array}{c|c} (1/\sqrt{2}) & (1/\sqrt{2}) \\ \hline (1/\sqrt{2}) & -1/\sqrt{2} \end{array} \right] \otimes \left[ \begin{array}{c|c} (1/\sqrt{2}) & (1/\sqrt{2}) \\ \hline (1/\sqrt{2}) & -1/\sqrt{2} \end{array} \right] = \left[ \begin{array}{c|c} \left( \begin{array}{c|c} 1/2 & 1/2 \\ \hline 1/2 & -1/2 \end{array} \right) & \left( \begin{array}{c|c} 1/2 & 1/2 \\ \hline 1/2 & -1/2 \end{array} \right) \\ \hline \left( \begin{array}{c|c} 1/2 & 1/2 \\ \hline 1/2 & -1/2 \end{array} \right) & \left( \begin{array}{c|c} -1/2 & -1/2 \\ \hline -1/2 & 1/2 \end{array} \right) \end{array} \right]$$

The above matrices have been separated into quadrants, and each quadrant represents a block. For the Hadamard matrices depicted, three of the four blocks are equal in both of the one-qubit matrices and also in the larger two-qubit matrix (the equivalent blocks are surrounded by parentheses). This repetition of equivalent blocks demonstrates that the tensor product of two equal matrices propagates block patterns. In the case of the above example, the pattern is that all but the lower-right quadrant of an  $n$ -qubit Hadamard operator are equal. Furthermore, the structure of the two-qubit matrix implies a recursive block sub-structure, which can be seen by recursively partitioning each of the quadrants in the two-qubit matrix:

$$\left[ \begin{array}{c|c} (1/\sqrt{2}) & (1/\sqrt{2}) \\ \hline (1/\sqrt{2}) & -1/\sqrt{2} \end{array} \right] \otimes \left[ \begin{array}{c|c} (1/\sqrt{2}) & (1/\sqrt{2}) \\ \hline (1/\sqrt{2}) & -1/\sqrt{2} \end{array} \right] = \left[ \begin{array}{c|c} \left( \begin{array}{c|c} (1/2) & (1/2) \\ \hline (1/2) & -1/2 \end{array} \right) & \left( \begin{array}{c|c} (1/2) & (1/2) \\ \hline (1/2) & -1/2 \end{array} \right) \\ \hline \left( \begin{array}{c|c} (1/2) & (1/2) \\ \hline (1/2) & -1/2 \end{array} \right) & \left( \begin{array}{c|c} (-1/2) & (-1/2) \\ \hline (-1/2) & 1/2 \end{array} \right) \end{array} \right]$$

The only difference between the values in the two-qubit matrix and the values in the one-qubit matrices is a factor of  $1/\sqrt{2}$ . Thus, we can recursively define the Hadamard operator as follows:

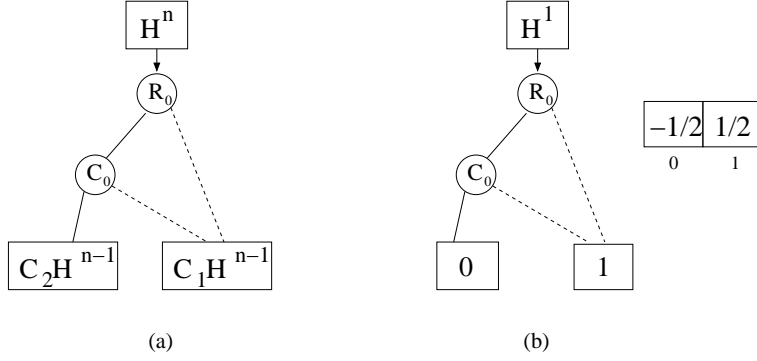


Figure 5: (a)  $n$ -qubit Hadamard QuIDD depicted next to (b) 1-qubit Hadamard QuIDD. Notice that they are isomorphic except at the terminals.

$$H^{n-1} \otimes H^{n-1} = \begin{bmatrix} C_1 H^{n-1} & C_1 H^{n-1} \\ C_1 H^{n-1} & C_2 H^{n-1} \end{bmatrix}$$

where  $C_1 = 1/\sqrt{2}$  and  $C_2 = -1/\sqrt{2}$ . Other operators constructed via the tensor product can also be defined recursively in a similar fashion.

Since three of the four blocks in an  $n$ -qubit Hadamard operator are equal, significant redundancy is exhibited. The interleaved variable ordering property allows a QuIDD to explicitly represent only two distinct blocks rather than four as shown in Figure 5. As we demonstrate in Sections 4 and 5, compression of equivalent block sub-structures using QuIDDs offers major performance improvements for many of the operators that are frequently used in quantum computation. In the next Subsection, we describe an algorithm which implements the tensor product for QuIDDs and leads to the compression just described.

### 3.3 Tensor Product

With the structure and variable ordering in place, operations involving QuIDDs can now be defined. Most operations defined for ADDs also work on QuIDDs with some modification to accommodate the QuIDD properties. The tensor (Kronecker) product has been described by Clarke et al. for MTBDDs representing various arithmetic transform matrices [6]. Here we reproduce an algorithm for the tensor product of QuIDDs based on the *Apply* operation that bears similarity to Clarke’s description. Recall that the tensor product  $A \otimes B$  produces a new matrix which multiplies each element of  $A$  by the entire matrix  $B$ . Rows (columns) of the tensor product matrix are component-wise products of rows (columns) of the argument matrices. Therefore it is straightforward to implement the tensor product operation on QuIDDs using the *Apply* function with an argument that directs *Apply* to multiply when it reaches the terminals of both operands. However, the main difficulty here lies in ensuring that the terminals of  $A$  are each multiplied by *all* the terminals of  $B$ . From the definition of the standard recursive *Apply* routine, we know that variables which precede other variables in the ordering are expanded first [5, 6]. Therefore, we must first shift all variables in  $B$  in the current order *after* all of the variables in  $A$  prior to the call to *Apply*. After this shift is performed, the *Apply* routine will then produce the desired behavior. *Apply* starts out with  $A * B$  and expands  $A$  alone until  $A_{terminal} * B$  is reached for each terminal in  $A$ . Once a terminal of  $A$  is reached,  $B$  is fully expanded, implying that each terminal of  $A$  is multiplied by all of  $B$ . The size of the resulting QuIDD and the runtime for generating it given two operands of sizes  $a$  and  $b$  (in number of nodes) is  $O(ab)$  because the tensor product simply involves a variable shift of complexity  $O(b)$ , followed by a call to *Apply*, which Bryant showed to have time and memory complexity  $O(ab)$  [5].

### 3.4 Matrix Multiplication

Matrix multiplication can be implemented very efficiently by using *Apply* to implement the dot-product operation. This follows from the observation that multiplication is a series of dot-products between the rows

of one operand and the columns of the other operand. In particular, given matrices  $A$  and  $B$  with elements  $a_{ij}$  and  $b_{ij}$ , their product  $C = AB$  can be computed element-wise by  $c_{ij} = \sum_{j=1}^n a_{ij}b_{ji}$ .

Matrix multiplication for QuIDDs is an extension of the *Apply* function that implements the dot-product. One call to *Apply* will not suffice because the dot-product requires *two* binary operations to be performed, namely addition and multiplication. To implement this we simply use the matrix multiplication algorithm defined by Bahar et al. for ADDs [2] but modified to support the QuIDD properties. The algorithm essentially makes two calls to *Apply*, one for multiplication and the other for addition.

Another important issue in efficient matrix multiplication is compression. To avoid the same problem that MATLAB encounters with its “packed” representation, ADDs do not require decompression during matrix multiplication. In the work of Bahar et al., this is addressed by tracking the number  $i$  of “skipped” variables between the parent node and its child node in each recursive call. To illustrate, suppose that  $\text{Var}(v_f) = x_2$  and  $\text{Var}(T(v_f)) = x_5$ . In this situation,  $i = 5 - 2 = 3$ . A factor of  $2^i$  is multiplied by the terminal-terminal product that is reached at the end of a recursive traversal [2].

The pseudo-code presented for this algorithm in subsequent work of Bahar et al. suggests time-complexity  $O((ab)^2)$  where  $a$  and  $b$  are the sizes, i.e., the number of decision nodes, of two ADD operands [2]. As with all BDD algorithms based on the *Apply* function, the size of the resulting ADD is on the order of the time complexity, meaning that the size is also  $O((ab)^2)$ . In the context of QuIDDs, we use a modified form of this algorithm to multiply operators by the state vector, meaning that  $a$  and  $b$  will be the sizes in nodes of a QuIDD matrix and QuIDD state vector, respectively. If either  $a$  or  $b$  or both are exponential in the number of qubits in the circuit, the QuIDD approach will have exponential time and memory complexity. However, in Section 4 we formally argue that many of the operators which arise in quantum computing have QuIDD representations that are polynomial in the number of qubits.

Two important modifications must be made to the ADD matrix multiply algorithm in order to adapt it for QuIDDs. To satisfy QuIDD properties 1 and 2, the algorithm must treat the terminals as indices into an array rather than the actual values to be multiplied and added. Also, a variable ordering problem must be accounted for when multiplying a matrix by a vector. A QuIDD matrix is composed of interleaved row and column variables, whereas a QuIDD vector only depends on column variables. If the ADD algorithm is run as described above without modification, the resulting QuIDD vector will be composed of row instead of column variables. The structure will be correct, but the dependence on row variables prevents the QuIDD vector from being used in future multiplications. Thus, we introduce a simple extension which transposes the row variables in the new QuIDD vector to corresponding column variables. In other words, for each  $R_i$  variable that exists in the QuIDD vector’s support, we map that variable to  $C_i$ .

### 3.5 Other Linear-Algebraic Operations

Matrix addition is easily implemented by calling *Apply* with *op* defined to be addition. Unlike the tensor product, no special variable order shifting is required for matrix addition. Another interesting operation which is nearly identical to matrix addition is element-wise multiplication  $c_{ij} = a_{ij}b_{ij}$ . Unlike the dot-product, this operation involves only products and no summation. This algorithm is implemented just like matrix addition except that *op* is defined to be multiplication rather than addition. In quantum computer simulation, this operation is useful for matrix-vector multiplications with a diagonal matrix like the Conditional Phase Shift in Grover’s algorithm [11]. Such a shortcut considerably improves upon full-fledged matrix multiplication. Interestingly enough, element-wise multiplication, and matrix addition operations for QuIDDs can perform, without the loss of efficiency, respective scalar operations. That is because a QuIDD with a single terminal node can be viewed both as a scalar value and as a matrix or vector with repeated values.

Since matrix addition, element-wise multiplication, and their scalar counterparts are nothing more than calls to *Apply*, the runtime complexity of each operation is  $O(ab)$  where  $a$  and  $b$  are the sizes in nodes of the QuIDD operands. Likewise, the resulting QuIDD has memory complexity  $O(ab)$  [5].

Another relevant operation which can be performed on QuIDDs is the transpose. It is perhaps the simplest QuIDD operation because it is accomplished by swapping the row and column variables of a QuIDD. The transpose is easily extended to the complex conjugate transpose<sup>1</sup> by first performing the transpose of a QuIDD and then conjugating its terminal values. The runtime and memory complexity of these operations

---

<sup>1</sup>The complex conjugate transpose is also known as the Hermitian conjugate or the adjoint.

is  $O(a)$  where  $a$  is the size in nodes of the QuIDD undergoing a transpose.

To perform quantum measurement (see Subsection 3.6) one can use the inner product, which can be faster than multiplying by projection matrices and computing norms. Using the transpose, the inner product can be defined for QuIDDs. The inner product of two QuIDD vectors, e.g.,  $\langle A|B\rangle$ , is computed by matrix multiplying the transpose of  $A$  with  $B$ . Since matrix multiplication is involved, the runtime and memory complexity of the inner product is  $O((ab)^2)$ , where  $a$  and  $b$  are the sizes in nodes of  $A$  and  $B$  respectively.

In our implementation, QuIDDPro, we currently support matrix multiplication, the tensor product, measurement, matrix addition, element-wise multiplication, scalar operations, the transpose, the complex conjugate transpose, and the inner product.

### 3.6 Measurement

Measurement can be defined for QuIDDs using a combination of operations. After measurement, the state vector is described by:

$$\frac{M_m|\psi\rangle}{\sqrt{\langle\psi|M_m^\dagger M_m|\psi\rangle}}$$

$M_m$  is a measurement operator and can be represented by a QuIDD matrix, and the state vector  $|\psi\rangle$  can be represented by a QuIDD vector. The expression in the numerator involves a QuIDD matrix multiplication. In the denominator,  $M_m^\dagger$  is the complex conjugate transpose of  $M_m$ , which is also defined for QuIDDs.  $M_m^\dagger M_m$  and  $M_m^\dagger M_m|\psi\rangle$  are matrix multiplications.  $\langle\psi|M_m^\dagger M_m|\psi\rangle$  is an inner product which produces a QuIDD with a single terminal node. Taking the square root of the value in this terminal node is straightforward. To complete the measurement, scalar division is performed with the QuIDD in the numerator and the single terminal QuIDD in the denominator as operands.

Let  $a$  and  $b$  be the sizes in nodes of the measurement operator QuIDD and state vector QuIDD, respectively. Performing the matrix multiplication in the numerator has runtime and memory complexity  $O((ab)^2)$ . The scalar division between the numerator and denominator also has the same runtime and memory complexity since the denominator is a QuIDD with a single terminal node. However, computing the denominator will have runtime and memory complexity  $O(a^{16}b^6)$  due to the matrix-vector multiplications and inner product.

## 4 Complexity Analyses

In this section we prove that the QuIDD data structure can represent a large class of state vectors and operators using an amount of memory that is *linear* in the number of qubits rather than exponential. Further, we prove that the QuIDD operations required in quantum circuit simulation, i.e., matrix multiplication, the tensor product, and measurement, have both runtime and memory that is linear in the number of qubits for the same class of state vectors and operators. In addition to these complexity issues, we also analyze the runtime and memory complexity of simulating Grover’s algorithm using QuIDDs.

### 4.1 Complexity of QuIDDs and QuIDD Operations

The key to analyzing the runtime and memory complexity of the QuIDD-based simulations lies in describing the mechanics of the tensor product. Indeed, the tensor product is the means by which quantum circuits can be represented with matrices. In the following analysis, the size of a QuIDD is represented by the number of nodes rather than actual memory consumption. Since the amount of memory used by a single QuIDD node is a constant, size in nodes is relevant for asymptotic complexity arguments. Actual memory usage in megabytes of QuIDD simulations is reported in Section 5.

Figure 6 illustrates the general form of a tensor product between two QuIDDs  $A$  and  $B$ .  $In(A)$  represents the internal nodes of  $A$ , while  $a_1$  through  $a_x$  denote terminal nodes. The notation for  $B$  is similar.

$In(A)$  is the root subgraph of the tensor product result because of the interleaved variable ordering defined for QuIDDs and the variable shifting operation of the tensor product (see Subsection 3.3). Suppose that  $A$  depends on the variables  $R_0 \prec C_0 \prec \dots \prec R_i \prec C_i$ , and  $B$  depends on the variables  $R_0 \prec C_0 \prec \dots \prec R_j \prec C_j$ . In performing  $A \otimes B$ , the variables on which  $B$  depends will be shifted to  $R_{i+1} \prec C_{i+1} \prec \dots \prec$

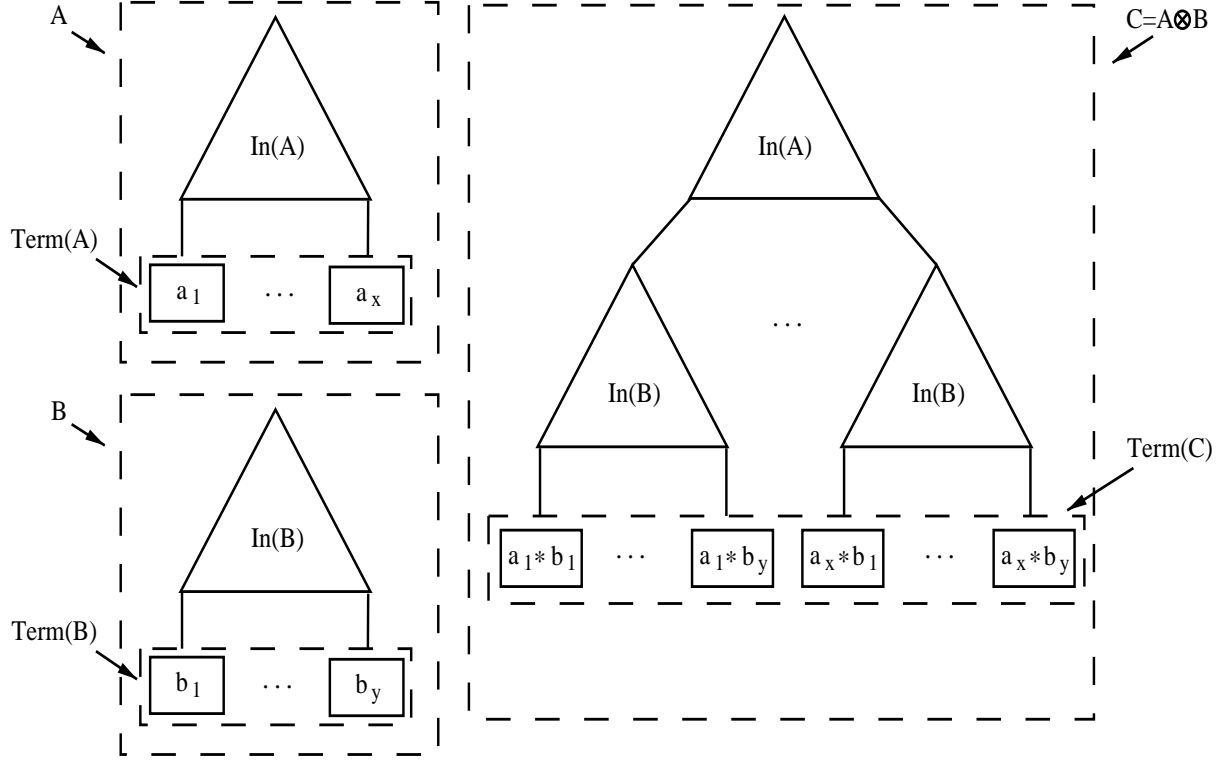


Figure 6: General form of a tensor product between two QuIDDs  $A$  and  $B$ .

$R_{k+i+1} \prec C_{k+i+1}$ . The tensor product is then completed by calling  $Apply(A, B, *)$ . Due to the variable shift on  $B$ , Rule 1 of the  $Apply$  function will be used after each comparison of a node from  $A$  with a node from  $B$  until the terminals of  $A$  are reached. Using Rule 1 for each of these comparisons implies that only nodes from  $A$  will be added to the result, explaining the presence of  $In(A)$ . Once the terminals of  $A$  are reached, Rule 2 of  $Apply$  will then be invoked since terminals are defined to appear last in the variable ordering. Using Rule 2 when the terminals of  $A$  are reached implies that all the internal nodes from  $B$  will be added in place of each terminal of  $A$ , causing  $x$  copies of  $In(B)$  to appear in the result (recall that there are  $x$  terminals in  $A$ ). When the terminals of  $B$  are reached, they are multiplied by the appropriate terminals of  $A$ . Specifically, the terminals of a copy of  $B$  will each be multiplied by the terminal of  $A$  that its  $In(B)$  replaced. The same reasoning holds for QuIDD vectors as vectors differ in that they depend only on  $R_i$  variables.

Figure 6 suggests that the size of a QuIDD constructed via the tensor product depends on the number of terminals in the operands. The more terminals a left-hand tensor operand contains, the more copies of the right-hand tensor operand's internal nodes will be added to the result. More formally, consider the tensor product of a series of QuIDDs  $\otimes_{i=1}^n Q_i = (\dots((Q_1 \otimes Q_2) \otimes Q_3) \otimes \dots \otimes Q_n)$ . Note that the  $\otimes$  operation is associative (thus parenthesis do not affect the result), but it is not commutative. The number of nodes in this tensor product is described by the following lemma.

**Lemma 4.1** *Given QuIDDs  $\{Q_i\}_{i=1}^n$ , the tensor-product QuIDD  $\otimes_{i=1}^n Q_i$  contains  $|In(Q_1)| + \sum_{i=2}^n |In(Q_i)| |Term(\otimes_{j=1}^{i-1} Q_j)| + |Term(\otimes_{i=1}^n Q_i)|$  nodes.<sup>2</sup>*

**Proof.** This formula can be verified by induction. For the base case,  $n = 1$ , there is a single QuIDD  $Q_1$ . Putting this information into the formula eliminates the summation term, leaving  $|In(Q_1)| + |Term(Q_1)|$  as the total number of nodes in  $Q_1$ . This is clearly correct since, by definition, a QuIDD is composed of its internal and terminal nodes. To complete the proof, we now show that if the formula is true for  $Q_n$  then it's true for  $Q_{n+1}$ . The inductive hypothesis for  $Q_n$  is  $|\otimes_{i=1}^n Q_i| = |In(Q_1)| + \sum_{i=2}^n |In(Q_i)| |Term(\otimes_{j=1}^{i-1} Q_j)| +$

<sup>2</sup> $|In(A)|$  denotes the number of internal nodes in  $A$ , while  $|Term(A)|$  denotes the number of terminal nodes in  $A$ .

$|Term(\otimes_{i=1}^n Q_i)|$ . For  $Q_{n+1}$  the number of nodes is:

$$\begin{aligned} & |(\otimes_{i=1}^n Q_i) \otimes Q_{n+1}| \\ &= |\otimes_{i=1}^n Q_i| - |Term(\otimes_{i=1}^n Q_i)| + |In(Q_{n+1})| |Term(\otimes_{i=1}^n Q_i)| + |Term(\otimes_{i=1}^{n+1} Q_i)| \end{aligned}$$

Notice that the number of terminals in  $\otimes_{i=1}^n Q_i$  are subtracted from the total number of nodes in  $\otimes_{i=1}^n Q_i$  and multiplied by the number of internal nodes in  $Q_{n+1}$ . The presence of these terms is due to Rule 2 of *Apply* which dictates that in the tensor-product  $(\otimes_{i=1}^n Q_i) \otimes Q_{n+1}$ , the terminals of  $\otimes_{i=1}^n Q_i$  are replaced by copies of  $Q_{n+1}$  where each copy's terminals are multiplied by a terminal from  $\otimes_{i=1}^n Q_i$ . The last term simply accounts for the total number of terminals in the tensor-product. Substituting the inductive hypothesis made earlier for the term  $|\otimes_{i=1}^n Q_i|$  produces:

$$\begin{aligned} & |In(Q_1)| + \sum_{i=2}^n |In(Q_i)| |Term(\otimes_{j=1}^{i-1} Q_j)| + |Term(\otimes_{i=1}^n Q_i)| - |Term(\otimes_{i=1}^n Q_i)| + \\ & |In(Q_{n+1})| |Term(\otimes_{i=1}^n Q_i)| + |Term(\otimes_{i=1}^{n+1} Q_i)| \\ &= |In(Q_1)| + \sum_{i=2}^{n+1} |In(Q_i)| |Term(\otimes_{j=1}^{i-1} Q_j)| + |Term(\otimes_{i=1}^{n+1} Q_i)| \end{aligned}$$

Thus the number of nodes in  $Q_{n+1}$  is equal to the original formula we set out to prove for  $n+1$  and the induction is complete.  $\square$

Lemma 4.1 suggests that if the number of terminals in  $\otimes_{i=1}^n Q_i$  increases by a certain factor with each  $Q_i$ , then  $\otimes_{i=1}^n Q_i$  must grow exponentially in  $n$ . If, however, the number of terminals stops changing, then  $\otimes_{i=1}^n Q_i$  must grow linearly in  $n$ . Thus, the growth depends on matrix entries because terminals of  $A \otimes B$  are products of terminal values of  $A$  by terminal values of  $B$  and repeated products are merged. If all QuIDDs  $Q_i$  have terminal values from the same set  $\Gamma$ , the product's terminal values are products of elements from  $\Gamma$ .

**Definition 4.2** Consider finite non-empty sets of complex numbers  $\Gamma_1$  and  $\Gamma_2$ , and define their *all-pairs product* as  $\{xy \mid x \in \Gamma_1, y \in \Gamma_2\}$ . One can verify that this operation is associative, and therefore the set  $\Gamma^n$  of all  $n$ -element products is well defined for  $n > 0$ . We then call a finite non-empty set  $\Gamma \subset \mathbb{C}$  *persistent* iff the size of  $\Gamma^n$  is constant for all  $n > 0$ .

For example, the set  $\Gamma = \{c, -c\}$  is persistent for any  $c$  because  $\Gamma^n = \{c^n, -c^n\}$ . In general any set closed under multiplication is persistent, but that is not a necessary condition. In particular, for  $c \neq 0$ , the persistence of  $\Gamma$  is equivalent to the persistence of  $c\Gamma$ . Another observation is that  $\Gamma$  is persistent if and only if  $\Gamma \cup \{0\}$  is persistent. An important example of a persistent set is the set consisting of 0 and all  $n$ -th degree roots of unity  $\mathbb{U}_n = \{e^{2\pi ik/n} \mid k = 0..n-1\}$ , for some  $n$ . Since roots of unity form a group, they are closed under multiplication and form a persistent set. In the Appendix, we show that every persistent set is either  $c\mathbb{U}_n$  for some  $n$  and  $c \neq 0$ , or  $\{0\} \cup c\mathbb{U}_n$ .

The importance of persistent sets is underlined by the following theorem.

**Theorem 4.3** Given a persistent set  $\Gamma$  and a constant  $C$ , consider  $n$  QuIDDs with at most  $C$  nodes each and terminal values from a persistent set  $\Gamma$ . The tensor product of those QuIDDs has  $O(n)$  nodes and can be computed in  $O(n)$  time.

**Proof.** The first and the last terms of the formula in Lemma 4.1 are bounded by  $C$  and  $|\Gamma|$  respectively. As the sizes of terminal sets in the middle term are bounded by  $|\Gamma|$ , the middle term is bounded by  $|\Gamma| \sum_{i=2}^n |In(Q_i)| < |\Gamma|c$  since each  $|In(Q_i)|$  is a constant. The tensor product operation  $A \otimes B$  for QuIDDs involves a shift of variables on  $B$  followed by *Apply*( $A, B, *$ ). If  $B$  is a QuIDD representing  $n$  qubits, then  $B$  depends on  $O(n)$  variables.<sup>3</sup> This implies that the runtime of the variable shift is  $O(n)$ . Bryant proved that the asymptotic runtime and memory complexity of *Apply*( $A, B, \text{binary\_op}$ ) is  $O(|A||B|)$  [5]. Lemma 4.1 and the fact that we are considering QuIDDs with at most  $C$  nodes and terminals from a persistent set  $\Gamma$  imply that  $|A| = O(n)$  and  $|B| = O(1)$ . Thus, *Apply*( $A, B, *$ ) has asymptotic runtime and memory complexity  $O(n)$ , leading to an overall asymptotic runtime and memory complexity of  $O(n)$  for computing  $\otimes_{i=1}^n Q_i$ .  $\square$

Importantly, the terminal values do not need to form a persistent set themselves for the theorem to hold. If they are *contained* in a persistent set, then the sets of all possible  $m$ -element products (i.e.  $m \leq n$  for

<sup>3</sup>More accurately,  $B$  depends on exactly  $2n$  variables if it is a matrix QuIDD and  $n$  variables if it is a vector QuIDD.

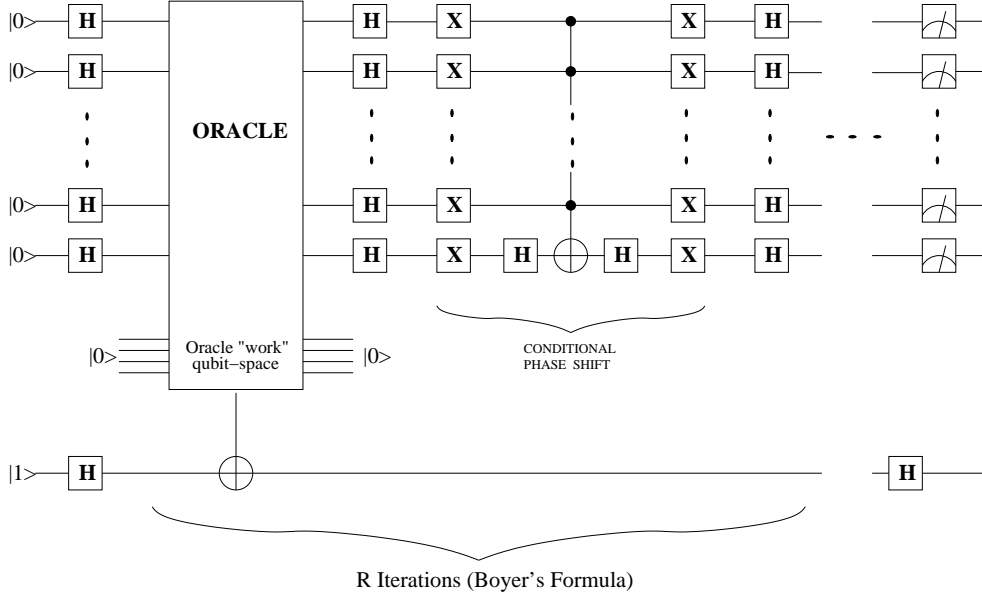


Figure 7: Circuit-level implementation of Grover's algorithm

all  $n$ -element products in a set  $\Gamma$ ) eventually stabilize in the sense that their sizes do not exceed that of  $\Gamma$ . However, this is only true for a fixed  $m$  rather than for the sets of products of  $m$  elements and fewer.

For QuIDDs  $A$  and  $B$ , the matrix-matrix and matrix-vector product computations are not as sensitive to terminal values, but depend on sizes of the QuIDDs. Indeed, the memory and time complexity of this operation is  $O(|A|^2|B|^2)$  [2].

**Theorem 4.4** Consider measuring an  $n$ -qubit QuIDD state vector  $|\psi\rangle$  using a QuIDD measurement operator  $M$ , where both  $|\psi\rangle$  and  $M$  are constructed via the tensor product of an arbitrary sequence of  $O(1)$ -sized QuIDD vectors and matrices, respectively. If the terminal node values of the  $O(1)$ -sized QuIDD vectors or operators are in a persistent set  $\Gamma$ , then the runtime and memory complexity of measuring the QuIDD state vector is  $O(n^{22})$ .

**Proof.** In Subsection 3.6, we showed that runtime and memory complexity for measuring a state vector QuIDD is  $O(a^{16}b^6)$ , where  $a$  and  $b$  be the sizes in nodes of the measurement operator QuIDD and state vector QuIDD, respectively. From Theorem 4.3, the asymptotic memory complexity of both  $a$  and  $b$  is  $O(n)$ , leading to an overall runtime and memory complexity of  $O(n^{22})$ .  $\square$

The class of QuIDDs described by Theorem 4.3 and its corollaries, with terminals taken from the set  $\{0\} \cup c\mathbb{U}$ , encompasses a large number of practical quantum state vectors and operators. These include, but are not limited to, any equal superposition of  $n$  qubits, any sequence of  $n$  qubits in the computational basis states,  $n$ -qubit Pauli matrices, and  $n$ -qubit Hadamard matrices. The above results suggest a polynomial-sized QuIDD representation of any quantum circuit on  $n$  qubits in terms of such gates if the number of gates is limited by a constant. In other words, the above sufficient conditions apply if the depth (length) of the circuit is limited by a constant. Our simulation technique may use polynomial memory and runtime in other circumstances as well, as shown in the next Subsection.

## 4.2 Complexity of Grover's Algorithm using QuIDDs

To demonstrate the power of our QuIDD representation, we used QuIDDPro to simulate Grover's algorithm [11], one of the two major quantum algorithms that have been developed to date. Grover's algorithm searches for a subset of items in an unordered database of  $N$  items. The only selection criterion available is a black-box predicate that can be evaluated on any item in the database. The complexity of this evaluation

(query) is unknown, and the overall complexity analysis is performed in terms of queries. In the classical domain, any algorithm for such an unordered search must query the predicate  $\Omega(N)$  times. However, Grover’s algorithm can perform the search with quantum query complexity  $O(\sqrt{N})$ , a quadratic improvement. This assumes that a quantum version of the search predicate can be evaluated on a superposition of all database items.

A quantum circuit representation of the algorithm involves five major components: an *oracle circuit*, a *conditional phase shift operator*, sets of Hadamard gates, the data qubits, and an oracle qubit. The oracle circuit is a Boolean predicate that acts as a filter, flipping the oracle qubit when it receives as input an  $n$  bit sequence representing the items being searched for. In quantum circuit form, the oracle circuit is represented as a series of controlled NOT gates with subsets of the data qubits acting as the control qubits and the oracle qubit receiving the action of the NOT gates. Following the oracle circuit, Hadamard gates put the  $n$  data qubits into an equal superposition of all  $2^n$  items in the database where  $2^n = N$ . Then a sequence of gates  $H^{\otimes n-1}CH^{\otimes n-1}$ , where  $C$  denotes the conditional phase shift operator, are applied iteratively to the data qubits. Each iteration is termed a *Grover iteration* [14].

Grover’s algorithm must be stopped after a particular number of iterations when the probability amplitudes of the states representing the items sought are sufficiently boosted. There must be enough iterations to ensure a successful measurement, but after a certain point the probability of successful measurement starts fading, and later changes periodically. In our experiments, we used the tight bound on the number of iterations formulated by Boyer et al. [4] when the number of solutions  $M$  is known in advance:  $\lfloor \pi/4\theta \rfloor$  where  $\theta = \sqrt{M/N}$ . The power of Grover’s algorithm lies in the fact that the data qubits store all  $N = 2^n$  items in the database as a superposition, allowing the oracle circuit to “find” all items being searched for *simultaneously*. A circuit implementing Grover’s algorithm is shown in Fig. 7. The algorithm can be summarized as follows:

Let  $N$  denote the number of elements in the database.

1. Initialize  $n = \lceil \log_2 N \rceil$  qubits to  $|0\rangle$  and the *oracle qubit* to  $|1\rangle$ .
2. Apply the Hadamard transform (H gate) to all qubits to put them into a uniform superposition of basis states.
3. Apply the oracle circuit. The oracle circuit can be implemented as a series of one or more CNOT gates representing the search criteria. The inputs to the oracle circuit feed into the control portions of the CNOT gates, while the oracle qubit is the target qubit for all of the CNOT gates. In this way, if the input to this circuit satisfies the search criteria, the state of the oracle qubit is flipped. For a superposition of inputs, those input basis states that satisfy the search criteria flip the oracle qubit in the composite state-space. The oracle circuit uses ancillary qubits as its workspace, reversibly returning them to their original states (shown as  $|0\rangle$  in Fig 7). These ancillary qubits will not be operated on by any other step in the algorithm.
4. Apply the H gate to all qubits except the oracle qubit.
5. Apply the *Conditional Phase-Shift* gate on all qubits except the oracle qubit. This gate negates the probability amplitude of the  $|000\dots 0\rangle$  basis state, leaving that of the others unaffected. It can be realized using a combination of X, H and  $C^{n-1}$ -NOT gates as shown. A decomposition of the  $C^{n-1}$ -NOT into elementary gates is given in [3].
6. Apply the H gate to all gates except the oracle qubit.
7. Repeat steps 3-6 (a single Grover iteration)  $R$  times, where  $R = \lfloor \frac{\pi}{4} \sqrt{\frac{N}{M}} \rfloor$  and  $M$  is the number of keys matching the search criteria [4].
8. Apply the H gate to the oracle qubit in the last iteration. Measure the first  $n$  qubits to obtain the index of the matching key with high probability.

Using explicit vectors and matrices to simulate the above procedure would incur memory and runtime complexities of  $\Omega(2^n)$ . However, this is not necessarily the case when using QuIDDs. To show this, we present a step-by-step complexity analysis for a QuIDD-based simulation of the procedure.

**Steps 1 and 2** Theorem 4.3 implies that the memory and runtime complexity of step 1 is  $O(n)$  because the initial state vector only contains elements in  $c\mathbb{U}_k \cup \{0\}$  and is constructed via the tensor product. Step 2 is simply a matrix multiplication of an  $n$ -qubit Hadamard matrix with the state vector constructed in step 1. The Hadamard matrix has memory complexity  $O(n)$  by Theorem 4.3. Since the state vector also has memory complexity  $O(n)$ , further matrix-vector multiplication in step 2 has  $O(n^4)$  memory and runtime

complexity because computing the product of two QuIDDs  $A$  and  $B$  takes  $O((|A||B|)^2)$  time and memory [2].

**Steps 3-6** In step 3, the state vector is matrix-multiplied by the oracle matrix. Again, the complexity of multiplying two arbitrary QuIDDs  $A$  and  $B$  is  $O((|A||B|)^2)$  [2]. The size of the state vector in step 3 is  $O(n^2)$ . If the size of the oracle is represented by  $|A|$ , then the memory and runtime complexity of step 3 is  $O((|A|n^4)^2)$ . Similarly, steps 4, 5, and 6 will have polynomial memory and runtime complexity in terms of  $|A|$  and  $n$ .<sup>4</sup> Thus we arrive at the  $O(|A|^{16}n^{32})$  worst-case upper-bound for the memory and runtime complexity of the simulation at step 6. Judging from our empirical data, this bound is typically very loose and pessimistic.

**Lemma 4.5** *The memory and runtime complexity of a single Grover iteration in a QuIDD-based simulation is  $O(|A|^{16}n^{32})$ .*

**Proof.** Steps 3 – 6 make up a single Grover iteration. Since the memory and runtime complexity of a QuIDD-based simulation after completing Step 6 is  $O(|A|^{16}n^{32})$ , the memory and runtime complexity of a single Grover iteration is  $O(|A|^{16}n^{32})$ .  $\square$

**Step 7** Step 7 does not involve a quantum operator, but rather it repeats a Grover iteration  $R = \lfloor \frac{\pi}{4} \sqrt{\frac{N}{M}} \rfloor$  times. As a result, Step 7 induces an exponential runtime for the simulation, since the number of Grover iterations is a function of  $N = 2^n$ . This is acceptable though because an actual quantum computer would also require exponentially many Grover iterations in order to measure one of the matching keys with a high probability [4]. Ultimately this is the reason why Grover’s algorithm only offers a *quadratic* and not an exponential speedup over classical search. Since Lemma 4.5 shows that the memory and runtime complexity of a single Grover iteration is polynomial in the size of the oracle QuIDD, one might guess that the memory complexity of Step 7 is exponential like the runtime. However, it turns out that the size of the state vector does not change from iteration to iteration, as shown below.

**Lemma 4.6** *The internal nodes of the state vector QuIDD at the end of any Grover iteration  $i$  are equal to the internal nodes of the state vector QuIDD at the end of Grover iteration  $i + 1$ .*

**Proof.** Each Grover iteration increases the probability of the states representing matching keys while simultaneously decreasing the probability of the states representing non-matching keys. Therefore, at the end of the first iteration, the state vector QuIDD will have a single terminal node for all the states representing matching keys and one other terminal node, with a lower value, for the states representing non-matching keys (there may be two such terminal nodes for non-matching keys, depending on machine precision). The internal nodes of the state vector QuIDD cannot be different at the end of subsequent Grover iterations because a Grover iteration does not change the pattern of probability amplitudes, but only their values. In other words, the same matching states always point to a terminal node whose value becomes closer to 1 after each iteration, while the same non-matching states always point to a terminal node (or nodes) whose value (or values) becomes closer to 0.  $\square$

**Lemma 4.7** *The total number of nodes in the state vector QuIDD at the end of any Grover iteration  $i$  is equal to the total number of nodes in the state vector QuIDD at the end of Grover iteration  $i + 1$ .*

**Proof.** In proving Lemma 4.6, we showed that the only change in the state vector QuIDD from iteration to iteration is the values in the terminal nodes (not the number of terminal nodes). Therefore, the number of nodes in the state vector QuIDD is always the same at the end of every Grover iteration.  $\square$

**Corollary 4.8** *In a QuIDD-based simulation, the runtime and memory complexity of any Grover iteration  $i$  is equal to the runtime and memory complexity of Grover iteration  $i + 1$ .*

**Proof.** Each Grover iteration is a series of matrix multiplications between the state vector QuIDD and several operator QuIDDs (Steps 3 – 6). The work of Bahar et al. shows that matrix multiplication with ADDs has runtime and memory complexity that is determined solely by the number of nodes in the operands (see

---

<sup>4</sup>As noted in step 5, the Conditional Phase-Shift operator can be decomposed into the tensor product of single qubit matrices, giving it memory complexity  $O(n)$ .

Section 3.4) [2]. Since the total number of nodes in the state vector QuIDD is always the same at the end of every Grover iteration, the runtime and memory complexity of every Grover iteration is the same.  $\square$

Lemmas 4.6 and 4.7 imply that Step 7 does not necessarily induce memory complexity that is exponential in the number of qubits. This important fact is captured in the following theorem.

**Theorem 4.9** *The memory complexity of simulating Grover’s algorithm using QuIDDs is polynomial in the size of the oracle QuIDD and the number of qubits.*

**Proof.** The runtime and memory complexity of a single Grover iteration is  $O(|A|^{16}n^{32})$  (Lemma 4.5), which includes the initialization costs of Steps 1 and 2. Also, the structure of the state vector QuIDD does not change from one Grover iteration to the next (Lemmas 4.6 and 4.7). Thus, the overall memory complexity of simulating Grover’s algorithm with QuIDDs is  $O(|A|^{16}n^{32})$ , where  $|A|$  is the number of nodes in the oracle QuIDD and  $n$  is the number of qubits.  $\square$

Other known simulation techniques have exponential memory complexity when simulating Grover’s algorithm. However, Theorem 4.9 implies that simulation using QuIDDs can offer *polynomial* memory complexity, and in fact, this is a pessimistic upper-bound. As we demonstrate experimentally in Section 5, for some oracles, simulating Grover’s algorithm with QuIDDs has memory complexity  $\Theta(n)$ . Furthermore, while other known simulation techniques applied to Grover’s algorithm have runtime complexity  $O(2^n)$ , simulation using QuIDDs has runtime complexity  $O(R|A|^{16}n^{32})$ , where  $R$  is the number of Grover iterations as defined earlier. This runtime complexity is the same as an actual, ideal quantum computer times a polynomial factor.

## 5 Empirical Validation

Implementation and validation is an important part of this work. This section describes issues that arise when designing an implementation and experimental results obtained from actual simulation.

### 5.1 Implementation Issues

Additional implementation details are required to fully support the QuIDD properties, including the use of complex arithmetic. Also, serious problems can arise if numerical precision is not accounted for. Here we discuss the design decisions we made with regards to these important issues.

**Complex Number Arithmetic.** At an abstract level, ADDs can support terminals of any numerical type, but CUDD’s implementation of ADDs does not. For efficiency reasons, CUDD stores node information in C *unions* which are interpreted numerically for terminals and as child pointers for internal nodes. However, it is well-known that unions are incompatible with the use of C++ classes because their multiple interpretations hinder the binding of correct destructors. In particular, complex numbers in C++ are implemented as a templated class and are incompatible with CUDD. This was one of the motivations for storing terminal values in an external array (QuIDD property 2).

**Numerical Precision.** Another important issue is the precision of complex numeric types. Over the course of repeated multiplications, the values of some terminals may become very small and induce round-off errors if the standard IEEE double precision floating-point types are used. This effect worsens for larger circuits. Unfortunately, such round-off errors can significantly affect the structure of a QuIDD by merging terminals that are only slightly different or not merging terminals whose values should be equal, but differ by a small computational error. The use of approximate comparisons with an epsilon works in certain cases but does not scale well, particularly for creating an equal superposition of states (a standard operation in quantum circuits). In an equal superposition, a circuit with  $n$  qubits will contain the terminal value  $\frac{1}{2^{n/2}}$  in the state vector. With the IEEE double precision floating-point type, this value will be rounded to 0 at  $n = 2048$ , preventing the use of epsilons for approximate comparison past  $n = 2048$ . Furthermore, a static value for epsilon will not work well for different sized circuits. For example,  $\epsilon = 10^{-6}$  may work well for  $n = 35$ , but not for  $n = 40$  because at  $n = 40$ , all values may be smaller than  $10^{-6}$ . Therefore, to address the problem of precision, QuIDDPro uses an arbitrary precision floating-point type from the GMP library [8] with the C++ complex template. Precision is then limited to the available amount of memory in the system.

Circuit Size $n$	Hadamards		Conditional Phase Shift	Oracles	
	Initial	Repeated		1	2
20	80	83	21	99	108
30	120	123	31	149	168
40	160	163	41	199	228
50	200	203	51	249	288
60	240	243	61	299	348
70	280	283	71	349	408
80	320	323	81	399	468
90	360	363	91	449	528
100	400	403	101	499	588

Table 1: Size of QuIDDs (# of nodes) for Grover’s algorithm.

## 5.2 Results for Simulating Grover’s Algorithm

Before starting simulation of an instance of Grover’s algorithm, we construct the QuIDD representations of Hadamard operators by incrementally tensoring together one-qubit versions of their matrices  $n - 1$  times to get  $n$ -qubit versions. All other QuIDD operators are constructed similarly. Table 1 shows sizes (in nodes) of respective QuIDDs at  $n$ -qubits, where  $n = 20..100$ . We observe that memory usage grows linearly in  $n$ , and as a result QuIDD-based simulations of Grover’s algorithm are not memory-limited even at 100 qubits. Note that this is consistent with Theorem 4.3.

With the operators constructed, simulation can proceed. Tables 2a and 2b show performance measurements for simulating Grover’s algorithm with an oracle circuit that searches for one item out of  $2^n$ . QuIDDPro achieves asymptotic memory savings compared to qubit-wise implementations (see Subsection 2.3) of Grover’s algorithm using Blitz++, a high-performance numerical linear algebra library for C++ [19], MATLAB, and Octave, a mathematical package similar to MATLAB. The overall runtimes are still exponential in  $n$  because Grover’s algorithm entails an exponential number of iterations, even on an actual quantum computer [4]. We also studied a “mod-1024” oracle circuit that searches for elements whose ten least significant bits are 1 (see Tables 3a and 3b). Results were produced on a 1.2GHz AMD Athlon with 1GB RAM running Linux. Memory usage for MATLAB and Octave is lower-bounded by the size of the state vector and conditional phase shift operator; Blitz++ and QuIDDPro memory usage is measured as the size of the entire program. Simulations using MATLAB and Octave past 15 qubits timed out at 24 hours.

## 5.3 Impact of Grover Iterations

To verify that the QuIDDPro simulation resulted in the exact number of Grover iterations required to generate the highest probability of measuring the items being sought as per the Boyer et al. formulation [4], we tracked the probabilities of these items as a function of the number of iterations. For this experiment, we used four different oracle circuits, each with 11,12, and 13 qubit circuits. The first oracle is called “Oracle N” and represents an oracle in which all the data qubits act as controls to flip the oracle qubit (this oracle is equivalent to Oracle 1 in the last subsection). The other oracle circuits are “Oracle N-1”, “Oracle N-2”, and “Oracle N-3”, which all have the same structure as Oracle N minus 1,2, and 3 controls, respectively. As described earlier, each removal of a control doubles the number of items being searched for in the database. For example, Oracle N-2 searches for 4 items in the data set because it recognizes the bit pattern  $111\dots1dd$ .

Table 4 shows the optimal number of iterations produced with the Boyer et al. formulation for all the instances tested. Figure 8 plots the probability of successfully finding any of the items sought against the number of Grover iterations. In the case of Oracle N, we plot the probability of measuring the single item being searched for. Similarly, for Oracles N-1, N-2, and N-3, we plot the probability of measuring any one of the 2, 4, and 8 items being searched for, respectively. By comparing the results in Table 4 with those in Figure 8, it can be easily verified that QuIDDPro uses the correct number of iterations at which measurement is most likely to produce items sought. Also notice that the probabilities, as a function of the number of iterations, follow a sinusoidal curve. It is therefore important to terminate at the exact optimal number of iterations not only from an efficiency standpoint but also to prevent the probability amplitudes of the items being sought from lowering back down toward 0.

Oracle 1: Runtime (s)				
$n$	Oct	MAT	B++	QP
10	80.6	6.64	0.15	0.33
11	2.65e2	22.5	0.48	0.54
12	8.36e2	74.2	1.49	0.83
13	2.75e3	2.55e2	4.70	1.30
14	1.03e4	1.06e3	14.6	2.01
15	4.82e4	6.76e3	44.7	3.09
16	> 24hrs	> 24hrs	1.35e2	4.79
17	> 24hrs	> 24hrs	4.09e2	7.36
18	> 24hrs	> 24hrs	1.23e3	11.3
19	> 24hrs	> 24hrs	3.67e3	17.1
20	> 24hrs	> 24hrs	1.09e4	26.2
21	> 24hrs	> 24hrs	3.26e4	39.7
22	> 24hrs	> 24hrs	> 24hrs	60.5
23	> 24hrs	> 24hrs	> 24hrs	92.7
24	> 24hrs	> 24hrs	> 24hrs	1.40e2
25	> 24hrs	> 24hrs	> 24hrs	2.08e2
26	> 24hrs	> 24hrs	> 24hrs	3.12e2
27	> 24hrs	> 24hrs	> 24hrs	4.72e2
28	> 24hrs	> 24hrs	> 24hrs	7.07e2
29	> 24hrs	> 24hrs	> 24hrs	1.08e3
30	> 24hrs	> 24hrs	> 24hrs	1.57e3
31	> 24hrs	> 24hrs	> 24hrs	2.35e3
32	> 24hrs	> 24hrs	> 24hrs	3.53e3
33	> 24hrs	> 24hrs	> 24hrs	5.23e3
34	> 24hrs	> 24hrs	> 24hrs	7.90e3
35	> 24hrs	> 24hrs	> 24hrs	1.15e4
36	> 24hrs	> 24hrs	> 24hrs	1.71e4
37	> 24hrs	> 24hrs	> 24hrs	2.57e4
38	> 24hrs	> 24hrs	> 24hrs	3.82e4
39	> 24hrs	> 24hrs	> 24hrs	5.64e4
40	> 24hrs	> 24hrs	> 24hrs	8.23e4

(a)

Oracle 1: Peak Memory Usage (MB)				
$n$	Oct	MAT	B++	QP
10	2.64e-2	1.05e-2	3.52e-2	9.38e-2
11	5.47e-2	2.07e-2	8.20e-2	0.121
12	0.105	4.12e-2	0.176	0.137
13	0.213	8.22e-2	0.309	0.137
14	0.426	0.164	0.559	0.137
15	0.837	0.328	1.06	0.137
16	1.74	0.656	2.06	0.145
17	3.34	1.31	4.06	0.172
18	4.59	2.62	8.06	0.172
19	13.4	5.24	16.1	0.172
20	27.8	10.5	32.1	0.172
21	55.6	NA	64.1	0.195
22	NA	NA	1.28e2	0.207
23	NA	NA	2.56e2	0.207
24	NA	NA	5.12e2	0.223
25	NA	NA	1.02e3	0.230
26	NA	NA	> 1.5GB	0.238
27	NA	NA	> 1.5GB	0.254
28	NA	NA	> 1.5GB	0.262
29	NA	NA	> 1.5GB	0.277
30	NA	NA	> 1.5GB	0.297
31	NA	NA	> 1.5GB	0.301
32	NA	NA	> 1.5GB	0.305
33	NA	NA	> 1.5GB	0.320
34	NA	NA	> 1.5GB	0.324
35	NA	NA	> 1.5GB	0.348
36	NA	NA	> 1.5GB	0.352
37	NA	NA	> 1.5GB	0.371
38	NA	NA	> 1.5GB	0.375
39	NA	NA	> 1.5GB	0.395
40	NA	NA	> 1.5GB	0.398

(b)

Table 2: Simulating Grover’s algorithm with  $n$  qubits using Octave (Oct), MATLAB (MAT), Blitz++ (B++) and our simulator QuIDDPro (QP). > 24hrs indicates that the runtime exceeded our cutoff of 24 hours. > 1.5GB indicates that the memory usage exceeded our cutoff of 1.5GB. Simulation runs that exceed the memory cutoff can also exceed the time cutoff, though we give memory cutoff precedence. NA indicates that after a cutoff of one week, the memory usage was still steadily growing, preventing a peak memory usage measurement.

## 6 Conclusions and Future Work

We proposed and tested a new technique for simulating quantum circuits using a data structure called a QuIDD. We have shown that QuIDDs enable practical, generic and reasonably efficient simulation of quantum computation. Their key advantages are faster execution and lower memory usage. In our experiments, QuIDDPro achieves exponential memory savings compared to other known techniques.

This result is a first step in part of our ongoing research which explores the *limitations* of quantum computing. Classical computers have the advantage that they are not subject to quantum measurement and errors. Thus, when competing with quantum computers, classical computers can simply run ideal error-free quantum algorithms (as we did in Section 5), allowing techniques such as QuIDDs to exploit the

Oracle 2: Runtime (s)				
$n$	Oct	MAT	B++	QP
13	1.39e3	1.31e2	2.47	0.617
14	3.75e3	7.26e2	5.42	0.662
15	1.11e4	4.27e3	11.7	0.705
16	3.70e4	2.23e4	24.9	0.756
17	> 24hrs	> 24hrs	53.4	0.805
18	> 24hrs	> 24hrs	1.13e2	0.863
19	> 24hrs	> 24hrs	2.39e2	0.910
20	> 24hrs	> 24hrs	5.15e2	0.965
21	> 24hrs	> 24hrs	1.14e3	1.03
22	> 24hrs	> 24hrs	2.25e3	1.09
23	> 24hrs	> 24hrs	5.21e3	1.15
24	> 24hrs	> 24hrs	1.02e4	1.21
25	> 24hrs	> 24hrs	2.19e4	1.28
26	> 24hrs	> 24hrs	> 1.5GB	1.35
27	> 24hrs	> 24hrs	> 1.5GB	1.41
28	> 24hrs	> 24hrs	> 1.5GB	1.49
29	> 24hrs	> 24hrs	> 1.5GB	1.55
30	> 24hrs	> 24hrs	> 1.5GB	1.63
31	> 24hrs	> 24hrs	> 1.5GB	1.71
32	> 24hrs	> 24hrs	> 1.5GB	1.78
33	> 24hrs	> 24hrs	> 1.5GB	1.86
34	> 24hrs	> 24hrs	> 1.5GB	1.94
35	> 24hrs	> 24hrs	> 1.5GB	2.03
36	> 24hrs	> 24hrs	> 1.5GB	2.12
37	> 24hrs	> 24hrs	> 1.5GB	2.21
38	> 24hrs	> 24hrs	> 1.5GB	2.29
39	> 24hrs	> 24hrs	> 1.5GB	2.37
40	> 24hrs	> 24hrs	> 1.5GB	2.47

(a)

Oracle 2: Peak Memory Usage (MB)				
$n$	Oct	MAT	B++	QP
13	0.218	8.22e-2	0.252	0.137
14	0.436	0.164	0.563	0.141
15	0.873	0.328	1.06	0.145
16	1.74	0.656	2.06	0.172
17	3.34	1.31	4.06	0.176
18	4.59	2.62	8.06	0.180
19	13.4	5.24	16.1	0.180
20	27.8	10.5	32.1	0.195
21	55.6	NA	64.1	0.199
22	NA	NA	1.28e2	0.207
23	NA	NA	2.56e2	0.215
24	NA	NA	5.12e2	0.227
25	NA	NA	1.02e3	0.238
26	NA	NA	> 1.5GB	0.246
27	NA	NA	> 1.5GB	0.256
28	NA	NA	> 1.5GB	0.266
29	NA	NA	> 1.5GB	0.297
30	NA	NA	> 1.5GB	0.301
31	NA	NA	> 1.5GB	0.305
32	NA	NA	> 1.5GB	0.324
33	NA	NA	> 1.5GB	0.328
34	NA	NA	> 1.5GB	0.348
35	NA	NA	> 1.5GB	0.352
36	NA	NA	> 1.5GB	0.375
37	NA	NA	> 1.5GB	0.375
38	NA	NA	> 1.5GB	0.395
39	NA	NA	> 1.5GB	0.398
40	NA	NA	> 1.5GB	0.408

(b)

Table 3: Simulating Grover’s algorithm with  $n$  qubits using Octave (Oct), MATLAB (MAT), Blitz++ (B++) and our simulator QuIDDPro (QP). > 24hrs indicates that the runtime exceeded our cutoff of 24 hours. > 1.5GB indicates that the memory usage exceeded our cutoff of 1.5GB. Simulation runs that exceed the memory cutoff can also exceed the time cutoff, though we give memory cutoff precedence. NA indicates that after a cutoff of one week, the memory usage was still steadily growing, preventing a peak memory usage measurement.

Oracle	11 Qubits	12 Qubits	13 Qubits
$N$	25	35	50
$N - 1$	17	25	35
$N - 2$	12	17	25
$N - 3$	8	12	17

Table 4: Number of Grover iterations at which Boyer et al. [4] predict the highest probability of measuring one of the items sought.

symmetries found in ideal quantum computation. On the other hand, quantum computation still has certain operators which cannot be represented using only polynomial resources on a classical computer, even with QuIDDs. Examples of such operators include the quantum Fourier Transform and its inverse which are used

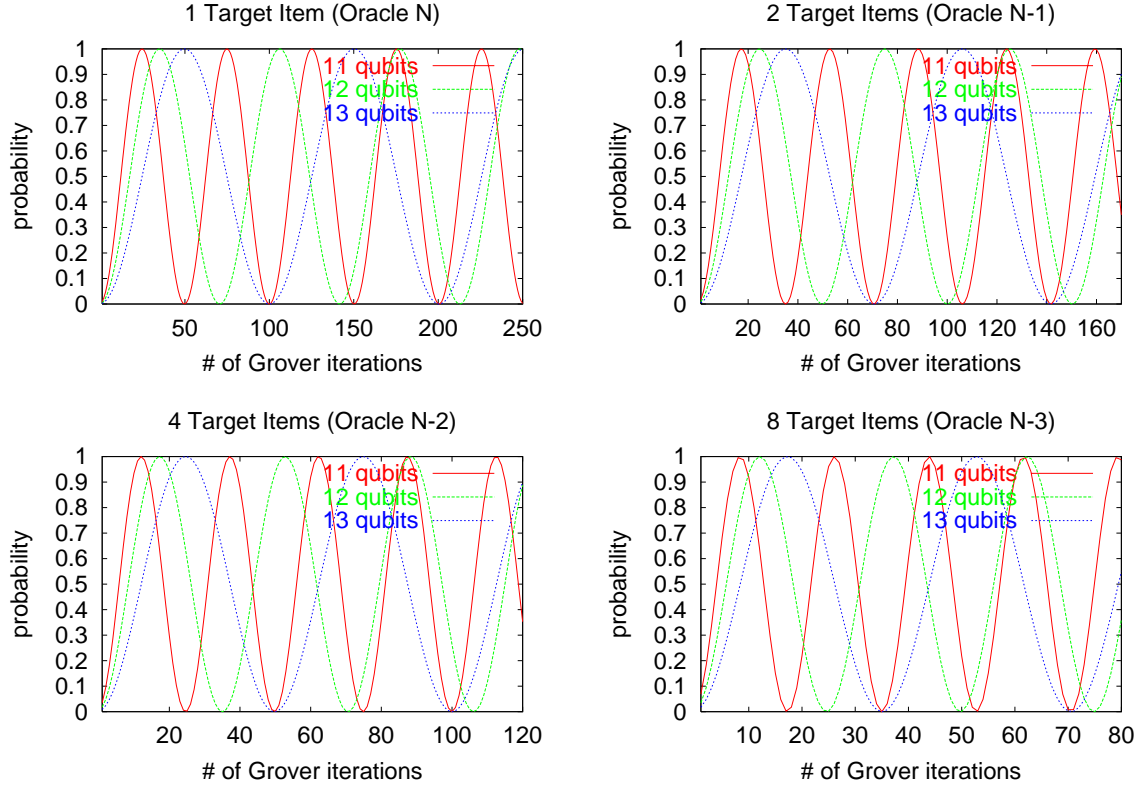


Figure 8: Probability of successful search for one, two, four and eight items as a function of the number of iterations after which the measurement is performed (11, 12 and 13 qubits). Note that the minima and maxima of the empirical sine curves match the predictions in Table 4.

in Shor’s number factoring algorithm [16]. Figure 9 shows the growth in number of nodes of the  $N$  by  $N$  inverse Fourier Transform as a QuIDD. Since  $N = 2^n$  where  $n$  is the number of qubits, this QuIDD exhibits exponential growth with a linear increase in qubits. Therefore, the Fourier Transform will cause QuIDDPro to have exponential runtime and memory requirements when simulating Shor’s algorithm. It is clear that there is still much work left to do with regards to more efficient classical simulation of quantum circuits.

Lastly, we are currently studying the growth of required precision and simulation of other aspects of quantum simulation including the effects of errors and decoherence. Error simulation is important if one plans to model actual quantum computational devices, and we suspect it may prove to be a difficult problem since errors may cause some of the symmetries exploited by QuIDDs to be lost.

## References

- [1] A. N. Al-Rabadi et al., “Multiple-Valued Quantum Logic,” *11th International Workshop on Post Binary ULSI*, Boston, MA., May 2002.
- [2] R. I. Bahar et al., “Algebraic Decision Diagrams and their Applications,” *Journal of Formal Methods in System Design*, Vol. 10, Number 2/3, April/May 1997.
- [3] A. Barenco et al., “Elementary gates for quantum computation”, *Los Alamos Quantum Physics Archive*, <http://xxx.lanl.gov/abs/quant-ph/9503016>, Mar. 1995.
- [4] M. Boyer, G. Brassard, P. Hoyer and A. Tapp, “Tight bounds on quantum searching,” *4th Workshop on Physics and Computation*, Nov. 1996.
- [5] R. Bryant, “Graph-Based Algorithms for Boolean Function Manipulation,” *IEEE Trans. on Computers*, Vol. C35, pp. 677-691, Aug 1986.

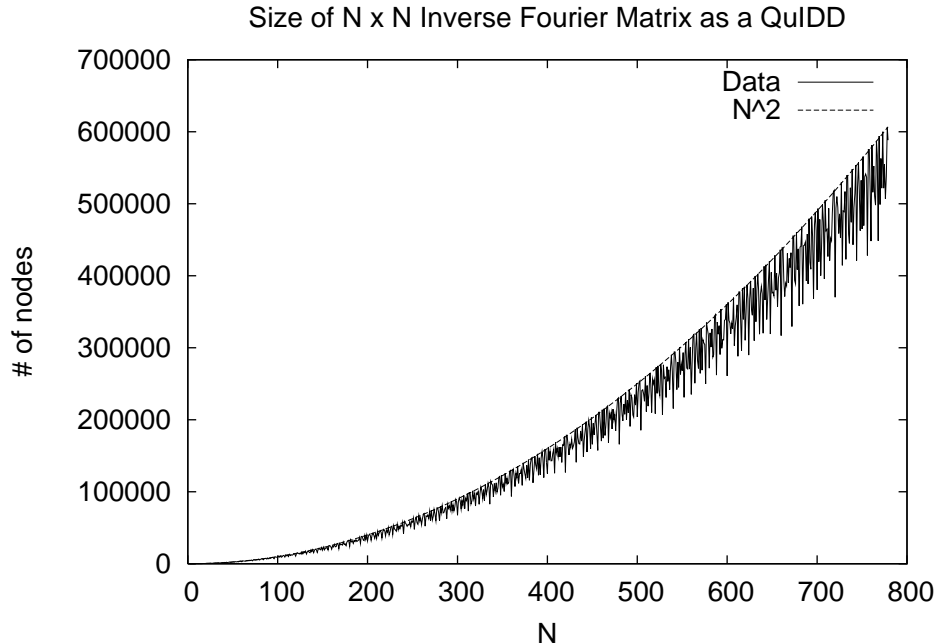


Figure 9: Growth of inverse Fourier Transform matrix in QuIDD form.  $N = 2^n$  for  $n$  qubits.

- [6] E. Clarke et al., “Multi-Terminal Binary Decision Diagrams and Hybrid Decision Diagrams,” in T. Sasao and M. Fujita, eds, *Representations of Discrete Functions*, pp. 93-108, Kluwer, 1996.
- [7] E. Clarke, M. Fujita, P. C. McGeer, K. McMillan, J. Yang, “Multi-Terminal Binary Decision Diagrams: An Efficient Data Structure for Matrix Representation,” *IWLS '93*, pp. 6a:1-15, May 1993.
- [8] “GNU MP (GMP): Arithmetic Without Limitations,” <http://www.swox.com/gmp/>
- [9] D. Gottesman, “The Heisenberg representation of quantum computers,” *Plenary speech at the 1998 International Conference on Group Theoretic Methods in Physics*, <http://xxx.lanl.gov/abs/quant-ph/9807006>.
- [10] D. Greve, “QDD: a quantum computer emulation library,” 1999 <http://thegreves.com/david/QDD/qdd.html>
- [11] L. Grover, “Quantum Mechanics Helps In Searching For A Needle In A Haystack,” *Phys. Rev. Lett.* (79), pp. 325-8, 1997.
- [12] A. J. G. Hey, ed., *Feynman and Computation: Exploring the Limits of Computers*, Perseus Books, 1999.
- [13] C.Y. Lee, “Representation of switching circuits by binary decision diagrams,” *Bell System Tech. J.*, Vol. 38, pp. 985-999, 1959.
- [14] M. A. Nielsen and I. L. Chuang, *Quantum Computation and Quantum Information*, Cambridge Univ. Press, 2000.
- [15] K. M. Obenland and A. M. Despain, “A Parallel Quantum Computer Simulator,” *High Performance Computing*, 1998.
- [16] P. W. Shor, “Polynomial-time algorithms for prime factorization and discrete logarithms on a quantum computer,” *SIAM J. of Computing*, Vol. 26, p. 1484, 1997.
- [17] F. Somenzi, “CUDD: CU Decision Diagram Package,” ver. 2.3.0, Univ. of Colorado at Boulder, 1998.
- [18] G. F. Viamontes, M. Rajagopalan, I. L. Markov and J. P. Hayes, “Gate-level Simulation of Quantum Circuits”, *In Proc. of ACM/IEEE Asia and South-Pacific Design Automation Conf. (ASPDAC)*, pp. 295-301, Kitakyushu, Japan, January 2003.
- [19] T. Veldhuizen, “Arrays in Blitz++”, in *Proc. 2nd Intl. Symp. on Computing in OO Parallel Environments*, 1998. <http://www.oonumerics.org/blitz/>

## Appendix: A Characterization of Persistent Sets

The following sequence of lemmas leads to a complete characterization of persistent sets from Definition 4.2. We start by observing that adding 0 to or removing 0 from a set does not affect its persistency.

**Lemma A.1** *Consider a persistent set  $\Gamma$  that does not contain 0. All of its elements must have the same magnitude.*

**Proof.** In order for  $\Gamma$  to be persistent, the set of magnitudes of elements from  $\Gamma$  must also be persistent. Therefore, it suffices to show that each persistent set of positive real numbers contains no more than one element. Assume, by contradiction, such a persistent set with at least two elements  $r$  and  $s$ . Then among  $n$ -element products from  $\Gamma$ , we find all numbers of the form  $r^{n-k}s^k$  for  $k = 0..n$ . If we order  $r$  and  $s$  so that  $r < s$ , then it becomes clear that they are all different because  $r^{n-k+1}s^{k-1} < r^{n-k}s^k$ .  $\square$

**Lemma A.2** *All persistent sets without 0 are of the form  $c\Gamma'$ , where  $c \neq 0$  and  $\Gamma'$  is a finite persistent subset of the unit circle in the complex plane, containing 1 and closed under multiplication. Vice versa, for all such sets  $\Gamma'$  and  $c \neq 0$ ,  $c\Gamma'$  is persistent.*

**Proof.** Take a persistent set  $\Gamma$  that does not contain 0, pick an element  $z \in \Gamma$  and define  $\Gamma' = \Gamma/z$ , which is persistent by construction.  $\Gamma'$  is a subset of the unit circle because all numbers in  $\Gamma$  have the same magnitude. Due to the fact that  $z/z = 1 \in \Gamma'$ , the set of  $n$ -element products contains every element of  $\Gamma'$ . Should the product of two elements of  $\Gamma'$  fall beyond the set,  $\Gamma'$  cannot be persistent.  $\square$

**Lemma A.3** *Finite subsets  $\Gamma$  of the unit circle, that are closed under multiplication and contain 1, map one-to-one to finite sets of real numbers from  $[0, 1]$  that are closed under addition modulo 1 and contain 0.*

**Proof.** For  $z \in \Gamma$ ,  $z \mapsto \log(z)/(2\pi i)$ . The inverse map:  $t \mapsto \exp(2\pi it)$ .  $\square$

**Lemma A.4** *In a subset of  $[0, 1]$  closed under addition modulo 1, the difference between any two numbers must be rational.*

**Proof** by contradiction. If  $a - b \bmod 1$  is irrational, then  $a + b \bmod 1$  is irrational. Then for any  $n$  and  $k$ , such that  $1 < k < n$ , all numbers  $(n-k)a + kb$  are different. Indeed, if two of them happen to be equal, this immediately gives a rational expression for  $a - b$ .

**Lemma A.5** *Each finite subset of  $[0, 1]$  closed under addition modulo 1 and containing 0 is of the form  $\{\frac{i}{n} \bmod 1\}_{i=0}^n$ , and this description is complete.*

**Proof.** Direct calculation shows that the given sets fit the bill. Vice versa, by an earlier result, all pairwise differences must be rational, thus all subset elements must be rational since 0 is in the subset. Consider the element  $i/n$  with the largest denominator  $n$ . Since its  $i$  is co-prime with  $n$ , this element generates the set  $\{\frac{i}{n} \bmod 1\}_{i=0}^n$  which must be contained in the subset. If the subset has more elements, their denominators cannot divide  $n$ . This leads to a contradiction because we can produce numbers in the subset with larger denominators than  $n$  by adding them to  $\frac{1}{n}$ .  $\square$

The following corollary and theorem follow from the previous lemmas.

**Corollary A.6** *Persistent subsets of the unit circle are of the form  $c\mathbb{U}_n$ .*

**Theorem A.7** *Persistent sets are either of the form  $c\mathbb{U}_n$  for some  $c \neq 0$  and  $n$ , or  $\{0\} \cup c\mathbb{U}_n$ .*